



Research Paper

Optimum design of ablative thermal protection systems for atmospheric entry vehicles



Aniello Riccio^a, Francesco Raimondo^a, Andrea Sellitto^a, Valerio Carandente^{b,*}, Roberto Scigliano^b, Domenico Tescione^b

^a Department of Industrial and Information Engineering, Second University of Naples, Italy

^b Structures and Materials Department, Italian Aerospace Research Centre (CIRA), Italy

HIGHLIGHTS

- Implement a FEM based model for the thermal analysis of ablative TPSs.
- Present an optimization procedure for the design of ablative heat shields.
- Apply the numerical method to the ablative TPS of the reentry capsule Stardust.

ARTICLE INFO

Article history:

Received 8 January 2016

Revised 3 March 2017

Accepted 11 March 2017

Available online 20 March 2017

Keywords:

TPS

Ablative materials

Thermal analysis

FEM

Optimization

ABSTRACT

The Thermal Protection System (TPS) provides spacecrafts entering the atmosphere with the thermal insulation from the aerothermodynamic heating. The design of such a subsystem is very critical, considering that its damage can lead to a catastrophic failure of the whole entry system, in particular if ablative materials are considered. In order to design an ablative TPS, in fact, a reliable numerical procedure, able to compute surface recession rate, pyrolysis and internal temperature histories under severe heating conditions, is necessary. Indeed, the TPS needs to be sized to effectively shield the spacecraft from the high heat fluxes acting during the atmospheric entry phase. At the same time, its weight has to be the minimum value able to guarantee a suitable protection.

This article aims to describe an optimization procedure for the design of ablative heat shields. In particular, in the present work, the numerical method is applied to the ablative TPS of the hypersonic reentry capsule Stardust.

© 2017 Elsevier Ltd. All rights reserved.

1. Introduction

During the atmosphere entry, hypersonic vehicles are subjected to strong shocks, equilibrium or non-equilibrium gas chemistry, large heat fluxes, and, as consequence, very high temperatures are reached on the structure. Those conditions require a proper designed Thermal Protection System (TPS). For very high entry speeds, in particular, the use of ablative material is mandatory. To design an ablative TPS, a reliable numerical procedure is needed to compute surface recession rate, pyrolysis effects, and internal temperature histories under severe heating conditions. As can be seen from a historical literature overview, considering the complex phenomenology of the ablative process, numerical models that can

describe this phenomenon are still in development [1,2]. The complexity of the phenomena under considerations is remarked by the unsatisfying analytical methods proposed [3,4]. Moreover, in the experimental field, tests are not easy to implement considering the complex environmental conditions encountered. Thus far, the most complete methodology for dealing with the problems related to ablation is the numerical resolution of differential equations governing the phenomena of interest. For this purpose, one possible approach assumes that the solid decomposes if a critical temperature is reached. This critical temperature is a material property and it is independent from the incoming heat flow. A further approach considers the chemical reactions in the char layer according to the “frozen chemistry” model or the “chemical equilibrium” model [5]. Despite the wide amount of research carried out so far, the design methodologies of ablative heat shields need not-negligible improvements. A fundamental aspect that these methods have to consider is related to the fact that the TPS usually

* Corresponding author at: Structures and Materials Department, Italian Aerospace Research Centre (CIRA), Via Maiorise snc, 81043 Capua, Italy.

E-mail address: valerio_carandente@hotmail.it (V. Carandente).

represents a large fraction of the total spacecraft volume [6]. The objective of this work is to estimate the heat shield minimum volume able to keep the mission requirements for a blunt-nosed sphere-conic capsule. The capsule in exam is in particular the Stardust probe. Stardust mission was the first U.S. mission solely dedicated to a comet study and was the first to return to Earth in 2006 cosmic dust and samples from a well-preserved comet called Wild-2 [7]. The heat shield of this probe was composed by a material called PICA (Phenolic Impregnated Carbon Ablator), which is part of the Lightweight Ceramic Ablators (LCAs) family. This material consists of a commercially available middle density carbon fiber matrix substrate impregnated with a phenolic resin [8].

The work is organized as follows. In Section 2 the theoretical background for the ablative phenomena, ablative classification and optimization process are presented. Section 3 reports the numerical model implemented. In Section 4, the results are illustrated and properly commented. Section 5 reports the main conclusions of the work.

2. Theoretical background

The TPS is a subsystem providing protection and insulation to a spacecraft from the aerodynamic heating due to high enthalpy flows encountered in the atmospheric entry phase at hypersonic speeds. Thermal protection systems for spacecrafts make use of different physicochemical mechanisms for their thermal energy management: dissipation, cooling, insulation and ablation. Leaving aside the isolation and cooling mechanisms, the heat shields can be divided into two big categories: reusable and ablative.

The reusable TPSs do not change the mass and composition of materials during the exposure to the aerothermodynamic environment. Their effectiveness is based partially on the absorption and partially on the re-radiation of the incoming heat flux. This feature guarantees the possibility to reuse these materials for different missions. Such systems, however, are utilized for relatively low thermal loads. The main characteristic of such heat shields is to re-radiate a large part of the energy coming from the convective and the radiative components of the aerothermodynamic heat flux, and to accommodate only a relatively small amount of energy by conduction within the material. Another key factor is linked to the use of insulating materials. They are often inorganic because of their low thermal conductivity and the need to minimize the overall mass of the heat shield [9].

The term “ablative” refers to a number of physicochemical processes, including vaporization, chemical reactions and erosion, leading to the surface material removal. For this class of materials, the incoming thermal loads are restrained thanks to the phase change of the material [10]. A classification from a phenomenological point of view divides ablative materials in two classes: non-charring and charring [11,12]. The charring type ablatives are best used for atmospheric entry missions. In this class, once the resin is heated, a decomposition phenomenon called pyrolysis takes place in the bulk of the material. The pyrolysis generates gaseous products, usually hydrocarbons, which blow through the heated surface into the boundary layer, with the consequent reduction of the effective convective flux affecting the spacecraft. The pyrolysis of the resin also produces a carbonaceous residue (char), which is deposited on the composite fibrous reinforcement. Moreover, the chemical reactions between the material at the surface and the boundary layer species can lead to a recession of the aforesaid material surface. These reactions can be endothermic (vaporization, sublimation) or exothermic (oxidation). The interaction of the ablative materials and their products with the ambient gases is much more complex than here described. On the other hand, in a non-charring type ablative, no internal pyrolysis phenomena

are encountered, but reactions are exclusively localized on the surface of the material [13]. In conclusion, ablation performs its function of thermal barrier through the dissipation of the incoming thermal energy thanks to the “sacrifice” of a part of the protecting material, which absorbs a considerable amount of heat and, at the same time, creates a barrier effect due to the generated gas flow. A further classification can be made according to the operating performance of the surface layer: “melting” and “non-melting” [14]. The first type consists of thermoplastic materials: a liquid surface layer produced by fusion is removed immediately by the aerodynamic shear stresses. The non-melting materials can be further divided into two sub-categories: “Low Temperatures Ablators” (LTA) and “High Temperatures Ablators” (HTA). The carbon-carbon and carbon-silicon ablatives are examples of HTA, whose main characteristic is to preserve mechanical properties even at high temperatures. For the LTAs, the chemical ablation is preceded by the deterioration of the mechanical properties with increasing temperature, while the thermal ablation (sublimation) becomes appreciable only from around 2500 K. This type of material is mainly used in return missions where very high heat fluxes are reached. An example of LTA is the ablative family consisting of carbon fibers and phenolic resins, such as PICA. They are recognizable for their excellent ability to form char and to ignite pyrolysis for high values of the heat flux.

The choice of an ablative material requires a careful evaluation of the entry conditions, looking for the best compromise between ablation effectiveness and heat insulation performance. In this way it is possible to identify the most fitting material for a particular mission.

The PICA is in particular a relatively new material, developed at NASA Ames Research Center, and is characterized by a lower-density value than other ablative materials, in particular with respect to the carbon phenolic, while maintaining a high ablative capacity for high heat fluxes [8]. Moreover, it presents a lower thermal conductivity of other ablative materials for same levels of incoming heat fluxes [8]. PICA is made with a thermosetting resin, a commercial phenol-formaldehyde (SC 1008) [15]. This resin acts as a matrix for carbon fibers chopped as shown in Fig. 1 [16].

It presents a final density of 0.22–0.32 g/cm³ and is characterized by the following mass composition: 92% carbon, 4.9% oxygen, 2.2% hydrogen and 0.9% nitrogen [17]. Its ablation rate increases with the incoming heat flow and the chemical species predominant in the char are C and CO. The high porosity possessed by such composite is the main reason for the low density and conductivity values. Complete properties of this material are reported in [8].

2.1. Physical phenomena in an ablative TPS

The ablation process involves multiple physical and chemical phenomena, in particular for charring type materials considered in this study. During hypersonic flight conditions, the formation of the bow shock, interacting with the boundary layer, leads to a temperature increase in the proximity of the vehicle surface. In addition to convective heating, and radiation produces non negligible effects, in particular at super-orbital entry speeds. This resulting heat flux is partially transferred by conduction within the material of the shield. For charring type materials, decomposition reactions originate gaseous products, leaving a carbonized porous residue. The pyrolysis gases originated by the underlying virgin material, generate a gaseous flow that, passing through the porous structure of the char, blows in the boundary layer. One of the effects of these gases is to reduce the effective convective heat flow acting on the TPS. On the other hand, these gases can trigger new corrosive processes due to their interaction with carbon residues. The carbonaceous residues may endure oxidation processes due

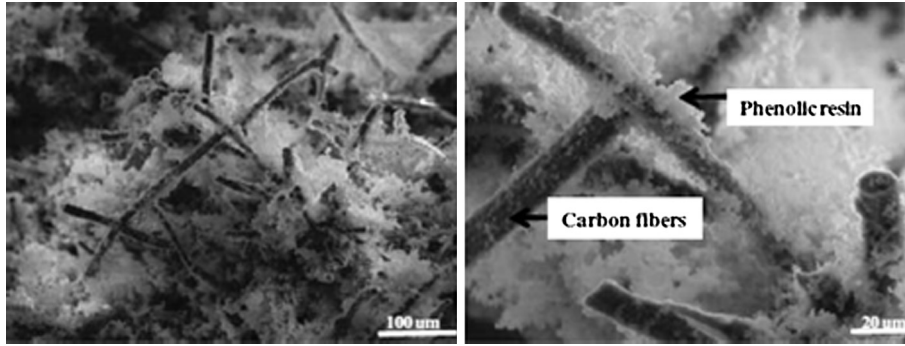


Fig. 1. Micrographs of PICA at different magnifications [16].

to the surrounding fluid and, finally, will also be present mechanical erosion phenomena. The consequence of all these phenomena is a thickness reduction of the ablative and shape variation of the heat shield. In conclusion, the ablation phenomenon consists into a number of physicochemical interaction between the TPS and the external environment.

2.2. Numerical model for thermal analyses

In the present work the complex physicochemical phenomena occurring in ablative TPSs are numerically modelled assuming a number of simplifying hypotheses, widely implemented in several works reported in literature [17–20]. As already discussed, PICA material is considered. Figs. 2–4 report thermal experimentally measured properties [8].

The material decomposition, or the density variation, is computed explicitly as a material property. The material density variation has been implemented applying the Arrhenius relation for each *i*th component of the PICA as in [18,19]. In Eq. (1), *B* and ψ are constants, *E* is the activation energy, ρ_0 and ρ_{ch} are the densities of the virgin and char material.

$$\frac{\partial \rho_i}{\partial t} = - \left(B_i \cdot e^{\frac{E_i}{RT}} \right) \cdot \rho_{0i} \cdot \left(\frac{\rho_i - \rho_{ci}}{\rho_{0i}} \right)^{\psi_i} \quad i = A, B, C \quad (1)$$

The values assumed for calculations are reported in Table 1.

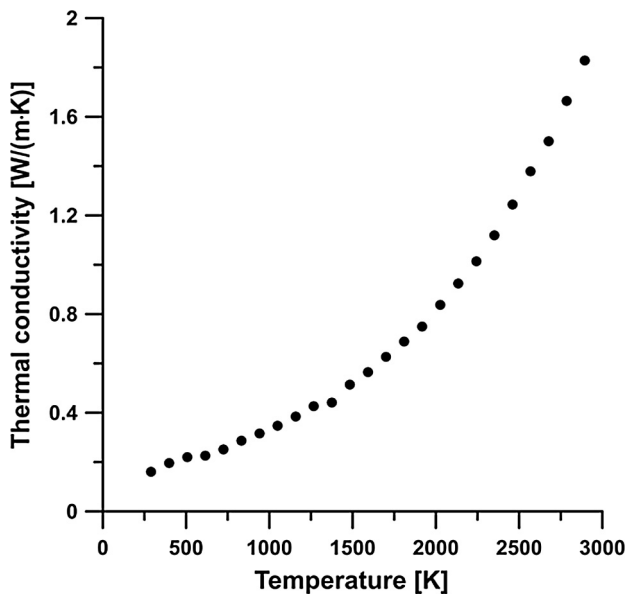


Fig. 2. PICA thermal conductivity as a function of the material temperature [8].

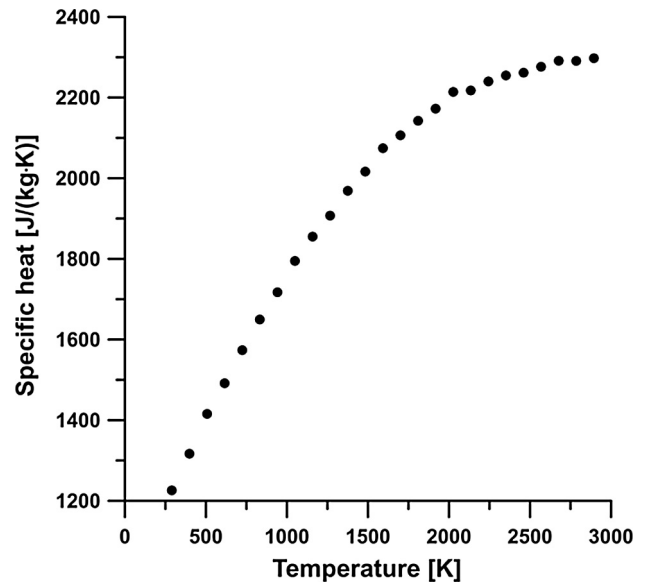


Fig. 3. PICA specific heat as a function of the material temperature [8].

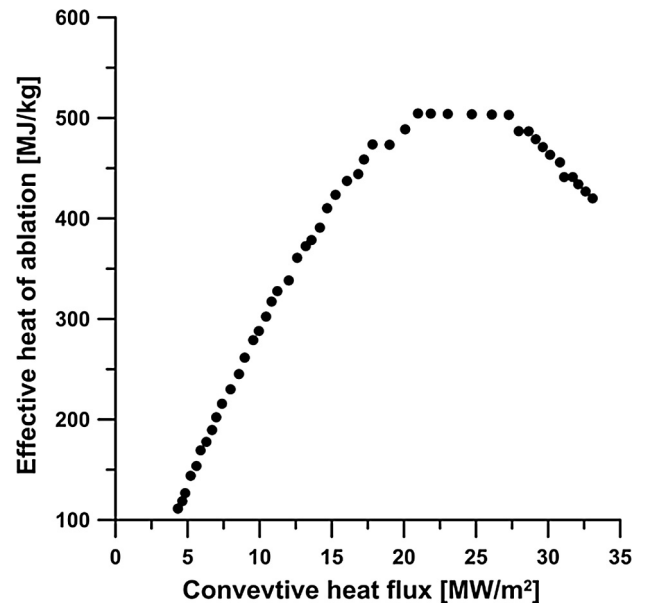


Fig. 4. PICA effective heat of ablation as a function of the convective heat flux acting on the material [8].

Table 1
Constant parameters implemented in Eq. (1).

Component	B (1/s)	Ψ (-)	E/R (K)	ρ_0 (kg/m ³)	ρ_c (kg/m ³)
A	1.40E4	3	8555.6	229	0
B	4.48E9	3	20444.4	972	792
C	0	0	0	160	160

The material density ρ has been therefore obtained as the weighted mean of its components (in Eq. (2)), Γ is the resin volume fraction, A and B represent the resin components and C the carbon Fiberform). These parameters have been set according to [18,20].

$$\rho = \Gamma(\rho_A - \rho_B) + (1 - \Gamma)\rho_C \quad (2)$$

The internal decomposition transforms part of the solid in pyrolysis gas. Moreover, thanks to the hypothesis of mono-dimensional flow, quasi-static and impermeability of the interface with the virgin material areas, the mass flow of the pyrolysis gas is connected to the decomposition by the simple relation reported as Eq. (3).

$$\frac{\partial \dot{m}_g}{\partial x} = \frac{\partial \rho}{\partial t} \quad (3)$$

According to the structure scheme reported in Fig. 5, the in-depth temperature response of the material has been carried out setting as boundary conditions the expressions reported in Eqs. (4–7). In particular, Eq. (4) refers to the external surface exposed to the aerothermodynamic environment ($y = h_i$). This approach has been widely discussed in [21].

$$\dot{q}_{in} = -k \left(\frac{\partial T}{\partial y} \right)_{y=h_i} = \dot{q}_{cw} \left(1 - \frac{c_p T_w}{H_{tot}} \right) \phi_{blow} - \sigma \varepsilon (T_w^4 - T_\infty^4) \quad (4)$$

$$\dot{q} = -k \left(\frac{\partial T}{\partial y} \right)_{y=0} = 0 \quad (5)$$

$$\dot{q} = -k \left(\frac{\partial T}{\partial x} \right)_{x=0} = 0 \quad (6)$$

$$\dot{q} = -k \left(\frac{\partial T}{\partial x} \right)_{x=b} = 0 \quad (7)$$

In Eq. (4), \dot{q}_{in} is the incoming net heat flux, \dot{q}_{cw} the cold wall convective heat flux, c_p is the specific heat at constant pressure, T_w the wall temperature, H_{tot} the total enthalpy, ϕ_{blow} the blowing coefficient,

calculated on the basis of the model reported in [13], σ the Stefan-Boltzmann constant, ε the material emissivity, T_∞ the asymptotic flow temperature.

As far as the material recession is concerned, the assumption of steady-state ablation has been considered. At each instant of time the ablation rate has been estimated by Eq. (9), in which Q^* is the so called heat of ablation, ρ is the material density and \dot{q}_{hw} is the hot wall convective heat flux, evaluated from Eq. (8) as:

$$\dot{q}_{hw} = \dot{q}_{cw} \left(1 - \frac{c_p T_w}{H_{tot}} \right) \quad (8)$$

$$\dot{s} = \frac{\dot{q}_{hw}}{\rho Q^*} \quad (9)$$

2.3. Verification and validation of the numerical model

As highlighted in [22] the main objective of the well-established Verification and Validation (V&V) methodology is to progress in the development of predictive numerical models. Oberkampf et al. [23] published a very detailed review paper about V&V. In this reference paper, the authors stated: “How should confidence in modelling and simulation be critically assessed? Verification and Validation (V&V) of computational simulations are the primary methods for building and quantifying this confidence”. In a paper dedicated to the relation between uncertainties and V&V for mechanics models, Thacker [24] presented also this process for the “development of models that can be used to make engineering predictions with high confidence”.

The verification phase deals with only numerical aspects. During the verification stage, one distinguishes between code verification and solution verification. Code verification leads to the identification of programming errors in the input and output data files, in the numerical algorithms, in the compilers and operating systems. The present study has been performed using Matlab [25] and APDL Ansys languages [26]. Therefore, code verification is assumed to be completed. As far as solution verification is concerned, the main source of errors is due to the spatial

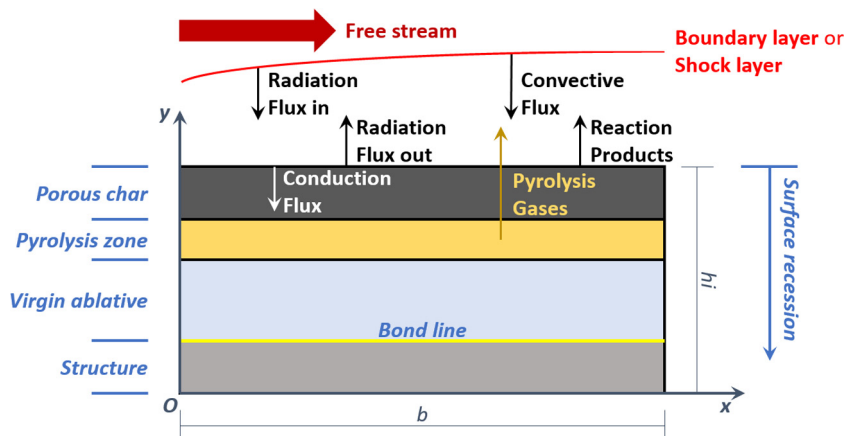


Fig. 5. Structure scheme and heat fluxes for charring ablative.

discretization. In order to ensure the time and mesh-independency a full convergence analysis has been performed on the model [21]. In addition, the model has been also validated crosschecking numerical results with analogous outcomes of experimental and numerical tests reported in literature [21,27].

For reader convenience, we briefly report, what is extensively presented in [21], i.e. a full convergence analysis realized reproducing the same experimental conditions adopted by Covington [27]. A cylindrical material sample geometry with a radius of 5.08 cm and an initial height of 2.74 cm has been taken into account with a material emissivity of 0.9 for the evaluation of the re-radiated heat flux. Reference test conditions are reported in Table 2, where t_{max} is the transient analysis duration.

The mesh has been realized using a growing number of elements in radial and axial directions, according to values reported in Table 3.

Two comparisons have been taken into account to evaluate the model robustness. The first is a comparison in terms of error of predicted final thickness and the second is in terms of final surface temperature.

In conclusion, results in terms of bulk and surface temperature can be considered sufficiently accurate even for a relatively low number of elements (Fig. 6), while a larger number of elements (Fig. 7) is required to increase accuracy on the discrete evaluation of the material thickness and to reduce the surface temperature drop connected with the element killing.

Finally, the results obtained with the $n = 100$ have been compared with both numerical and experimental results presented by Covington in [27] showing a very satisfying results cross-checking.

2.4. Optimization process

A genetic optimization procedure has been applied to the thermal protection shield in order to evaluate the minimum weight for the capsule TPS able to guarantee an effective thermal protection. Genetic Algorithms (GAs) fall within natural methods and can be used to solve problems of research and optimization. GAs are applicable to the resolution of a wide variety of problems not appropriate for classic optimization algorithms, including those in which the objective function is discontinuous, non-differentiable, stochastic, or strongly nonlinear [28–30].

GAs work with a population of individuals, each of which represents a possible solution of the analyzed problem. Each individual is assigned a score, called “fitness”, representing the goodness of the solution to the problem. The specimen with the best features (i.e. those with higher fitness values), have greater opportunity to “mate” with other individuals of the population that will generate other specimens of the population. If the resulting individuals have a sufficiently large fitness value, they will replace the worst individuals of the previous generation. In such a way, in the further generation there will be a higher number of characteristics possessed by the best individuals of the previous generation. This will ensure that the best features will be propagated to more individuals in the population. Moreover, features not included among those of the original genetic species can sporadically be created by the introduction of random mutations in the generation of new individuals. If the optimization is well designed, the population will converge to an optimal solution of the problem.

Table 2 Test condition for model verification and validation.

\dot{Q}_{cw} (MW/m ²)	p (atm)	H_{tot} (MJ/kg)	t_{max} (s)
5.80	0.450	29.5	15

Table 3 Number of elements in radial and axial directions for the different analyzed cases.

Case #	Number of elements	
	Axial direction (n)	Radial direction (m)
1	10	20
2	25	45
3	50	95
4	75	135
5	100	185

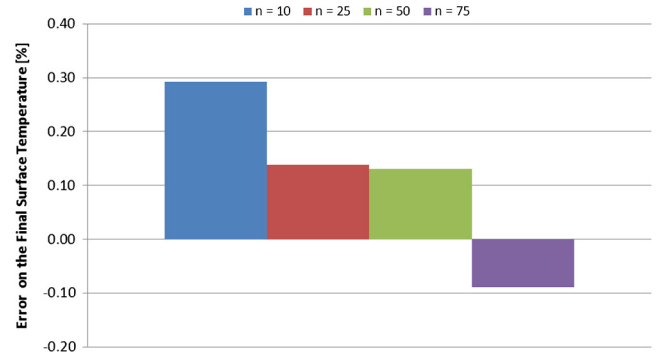


Fig. 6. Error on the final surface temperature for the analyzed cases.

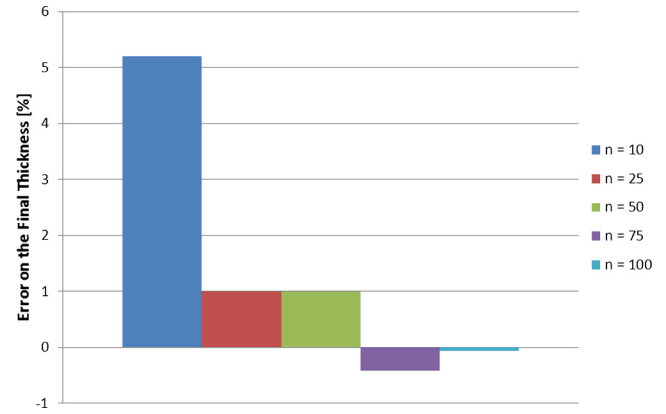


Fig. 7. Error on the final thickness for the analyzed cases.

3. Numerical modelling

Calculating the thermal response of an entry vehicle TPS is very important for its correct sizing. On one hand the instantaneous material recession rate has to be estimated and, on the other hand, the in-depth temperature response of the TPS has to be computed in order to evaluate the amount of material required as insulation to keep the bond-line temperature (i.e., the temperature of the material surface not directly exposed to the flow) below a specified limit.

In order to appreciate the material ablation of the external surface of the heat shield, a Finite Element Analysis has been performed within this work. An advanced finite element model has been introduced to predict the final thickness and shape of the heat shield, at the end of the atmospheric entry phase.

3.1. Analyzed geometry

In this work the Stardust probe has been analyzed. It has six major components: a heat shield, a back shell, a sample canister,

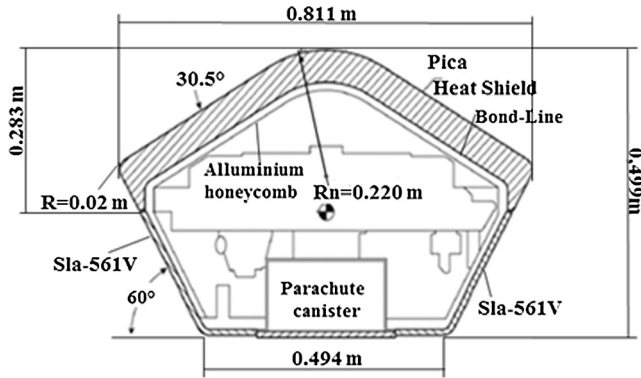


Fig. 8. Schematic diagram of the Stardust Sample Return Capsule (SRC) [31].

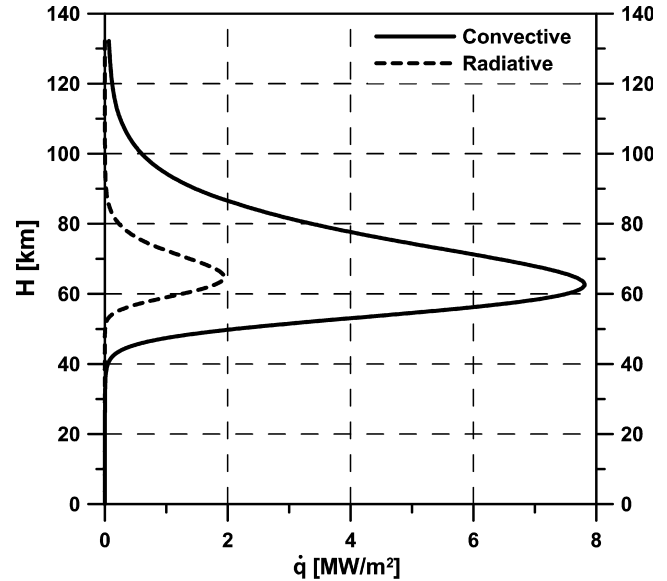


Fig. 10. Convective and radiative heat fluxes profiles estimated along the SRC entry trajectory.



Fig. 9. Geometry of the analyzed capsule in FE model.

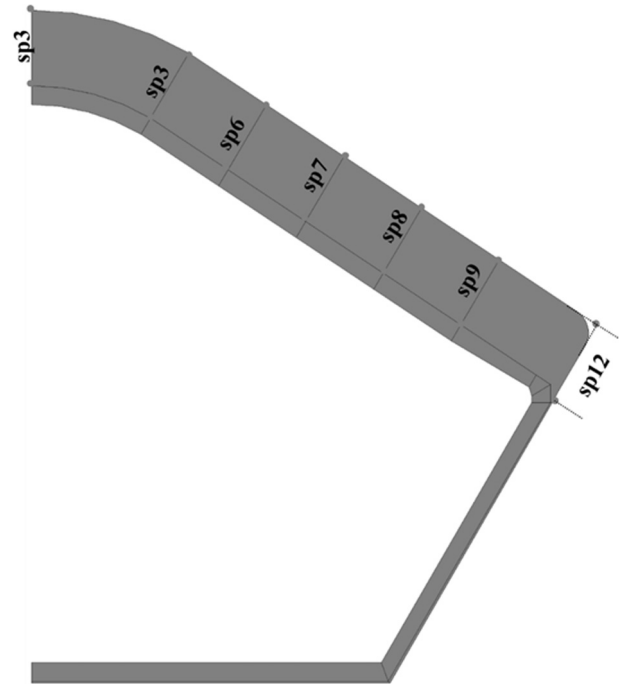


Fig. 11. Design variables.

a parachute system and avionics. The Stardust Return Capsule (SRC) is a short truncated cone, having a 0.811 m diameter, 0.499 m high and a total mass of 45.8 kg, including the parachute system [7]. In Fig. 8a 2D schematic diagram of the SRC is reported.

The geometry described above was discretized in the axisymmetric model depicted in Fig. 9.

The Ansys[®] Mechanical FE code [26] has been used to apply the numerical procedure hereinafter discussed to the computational mesh shown in Fig. 9. In particular, 2D elements PLANE55 have been selected to perform thermal calculations. Each element has four nodes with a single degree of freedom, the temperature, at each node.

3.2. Ablation and optimization modelling boundary conditions

The cold wall convective heat flux, the total enthalpy and the radiation flux profiles along the entry trajectory of the SRC have been imported as external arrays. In order to calculate these arrays,

it was necessary to numerically solve the equation characterizing the dynamics of the entry capsule [32], taking advantage of the Runge-Kutta method [33]. Once the data of the re-entry trajectory have been calculated, the convective heating at the stagnation-point of axisymmetric blunt bodies has been estimated by Sutton-Graves formulation [34]. This model is characterized by Eq. (10), according to [34], where V is the velocity in m/s, ρ is the atmospheric density in kg/m^3 , R_n is the nose radius in m and $1.73 \cdot 10^{-4}$ is a constant derived for the Earth atmosphere.

$$\dot{q}_{conv} = 1.73 \cdot 10^{-4} \cdot V^3 \sqrt{\frac{\rho}{R_n}} \quad (10)$$

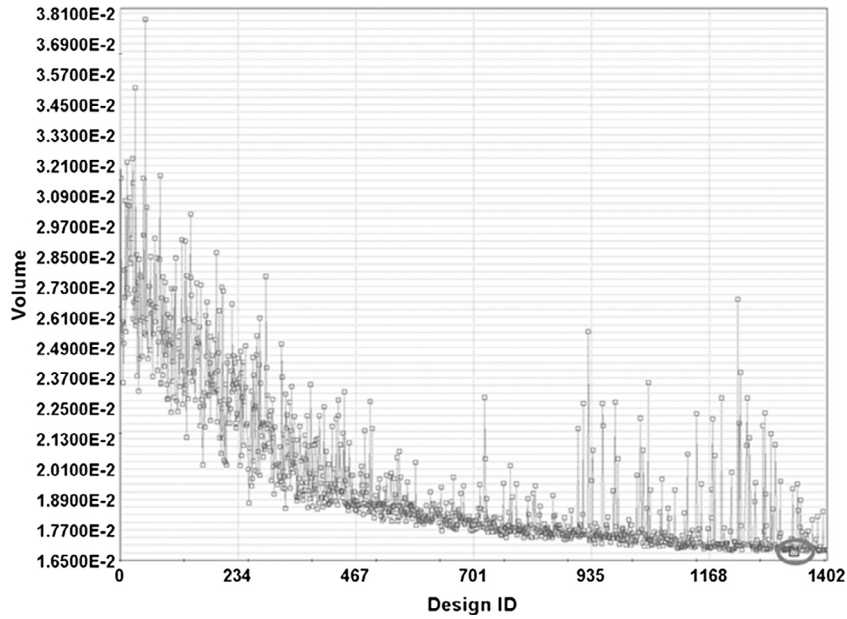


Fig. 12. Object function Vs ID number.

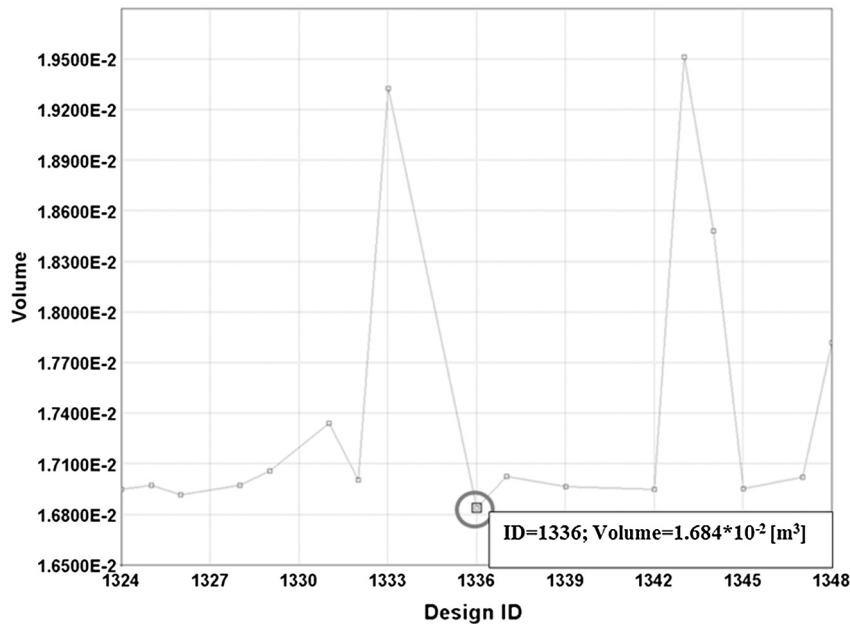


Fig. 13. Object function Vs ID number – Detail of the best ID.

However, convective heat flux is not the only thermal load acting on a re-entering capsule: radiative heat fluxes are also significant for the thermal protection system. Among the different engineering models for radiative heating available in literature, the one provided by Tauber and Sutton [35] has been considered in the present work. Tauber and Sutton’s engineering correlation is reported in Eq. (11), being C a constant that depends on the atmosphere and $f(V)$ tabulated values, functions of both flight velocities V and atmospheric composition. The exponents a and b can be either constants or functions of density and free stream velocity, as specified in [35].

$$\dot{q}_{rad} = CR_n^a \rho^b f(V) \tag{11}$$

In Fig. 10, convective and radiative heat fluxes at the stagnation point estimated along the SRC entry trajectory are shown.

A preliminary estimation, valid in hypersonic regime for high Mach numbers, of the non-dimensional heat flux distribution along the capsule surface has been obtained implementing the Lees’ theory [36]. The corresponding dimensional values have been obtained multiplying the non-dimensional heat flux spatial distribution by the temporal variation of the stagnation-point heat flux along the trajectory.

Once these arrays containing the external loads have been imported, the net heat flux is applied at each instant of time, taking into account the surface temperature calculated as solution of the thermal transient analysis at the previous time instant. For surface temperatures higher than a threshold value, the ablation rate \dot{s} has been estimated by Eq. (9), according to [8,18,21,34]. Then, the thickness of the heat shield is reduced of the quantity $\dot{s} \cdot dt$. When the thickness reduction is such that more than a half of an element

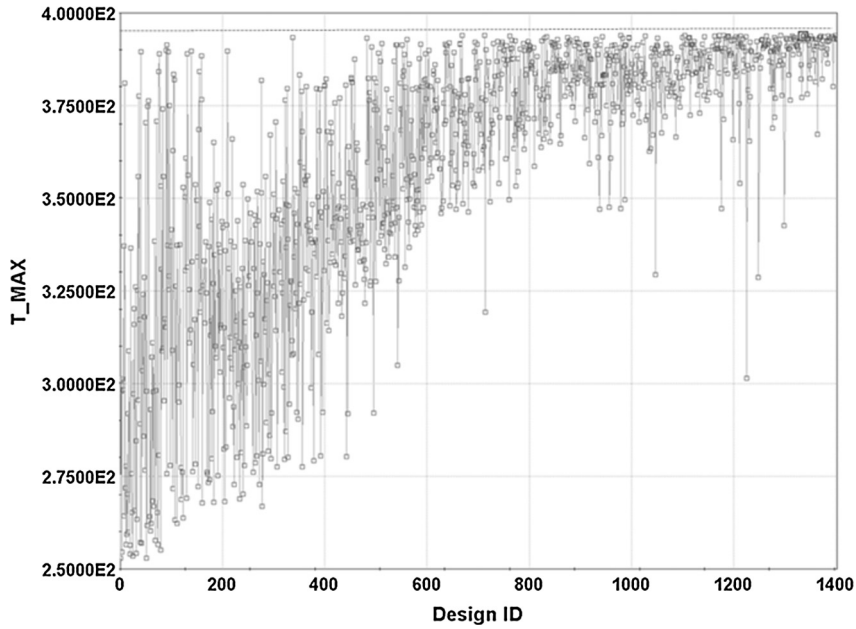


Fig. 14. Peak bond-line temperature Vs ID.

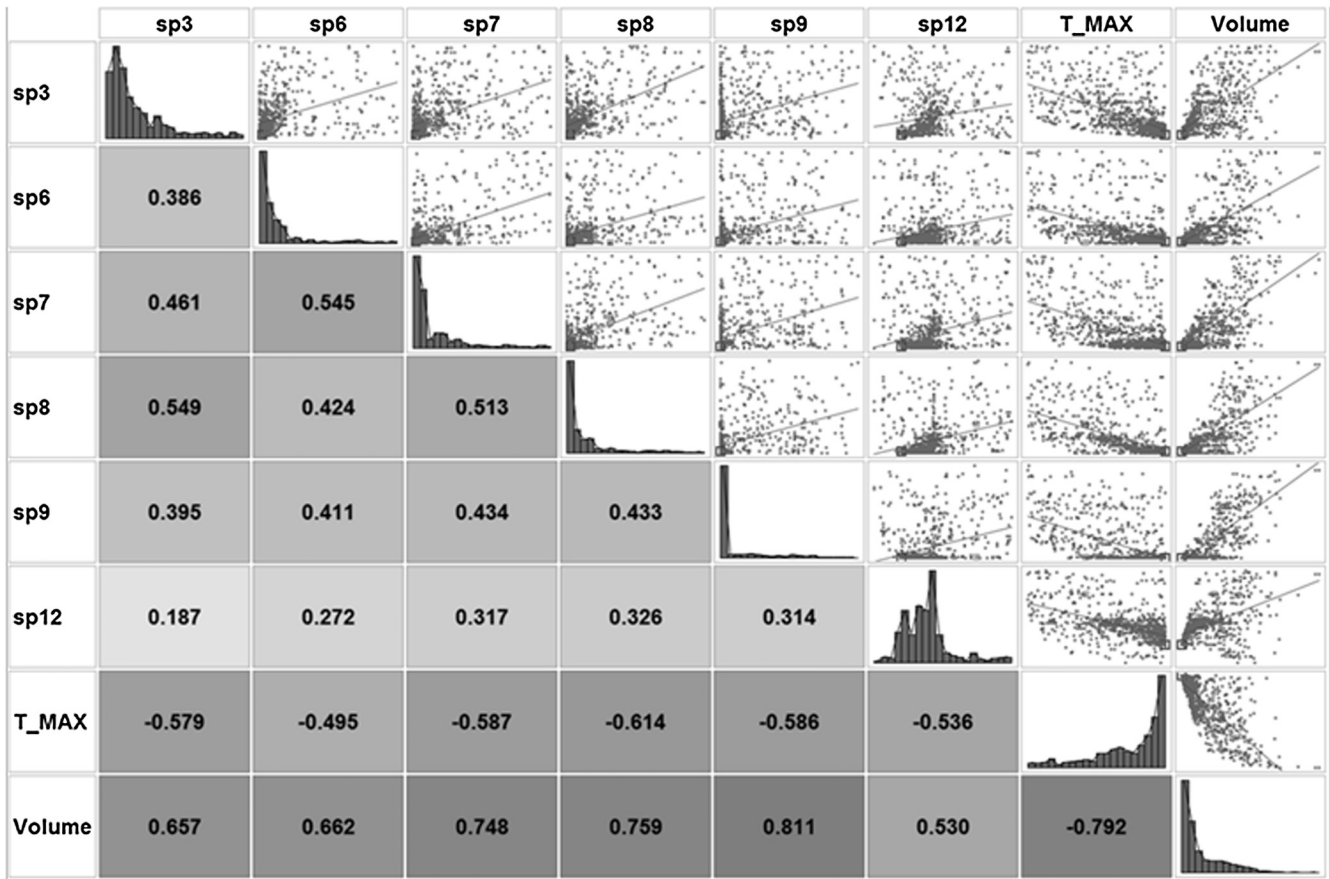


Fig. 15. Scatter Matrix.

thickness is not included in the computational domain, this element is disabled by the “ekill” function of the Ansys® code [26]. Once the analysis is completed, the value of the nodes temperature on the bond line are compared with the design limits [37,38].

This numerical model has been implemented in an optimization tool, allowing to obtain the configuration with the lowest ablative volume, while observing the temperature conditions of the bond-line [37,38]. In particular, this optimization process considers the



Fig. 16a. Initial computational mesh for ID 0.



Fig. 17a. Final computational mesh for ID 0.



Fig. 16b. Initial computational mesh for ID 1336.



Fig. 17b. Final computational mesh for ID 1336.

volume of the ablative shield as the object function, while the constraint function is the maximum temperature on the bond-line. An initial population of 50 individuals has been considered for the first generation, and a total of 50 generations have been analyzed. The choice of the first 50 individuals is based on a random sequence, filling randomly, with a uniform distribution, the design space [39].

Each individual of the population is described with six design variables. These variables represent the value of thickness of the PICA heat shield, measured starting from the bond line to the outer surface, in seven control points, as shown in Fig. 11.

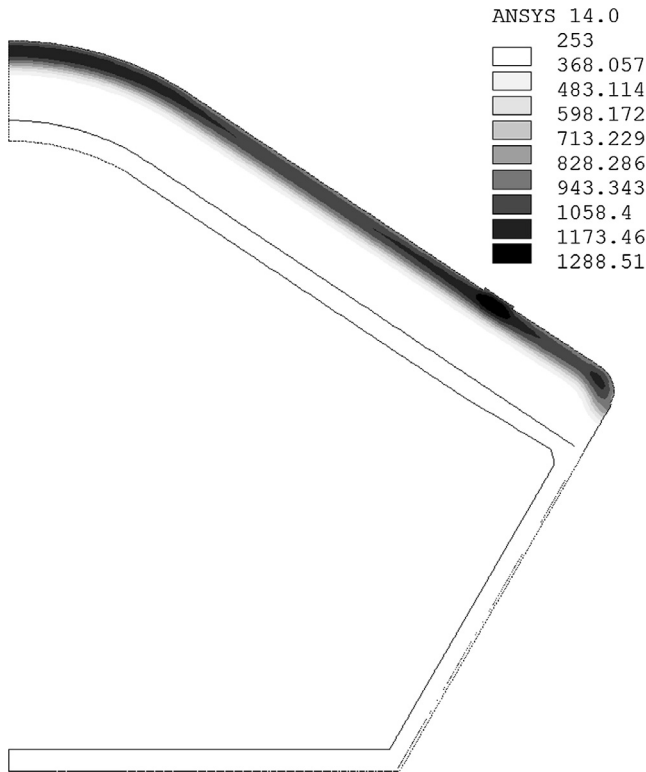


Fig. 18a. Final nodal temperature distribution for ID 0.

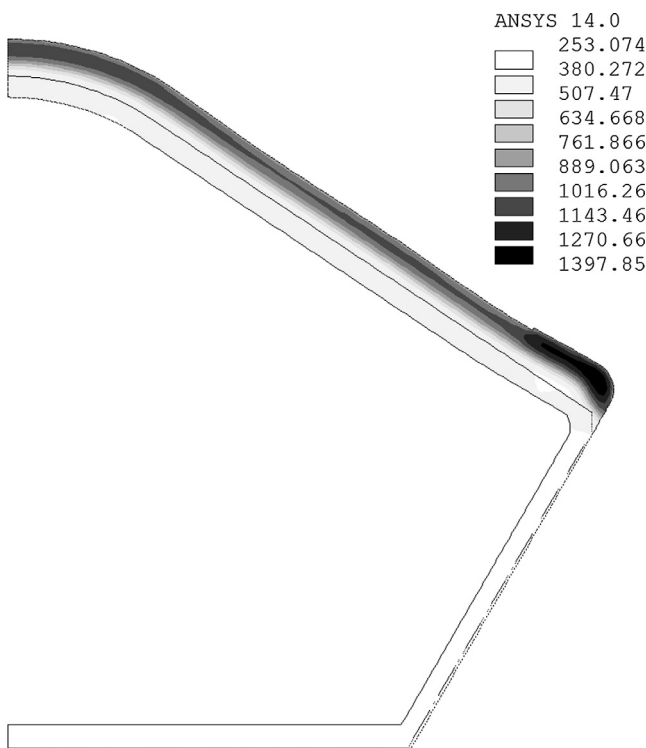


Fig. 18b. Final nodal temperature distribution for ID 1336.

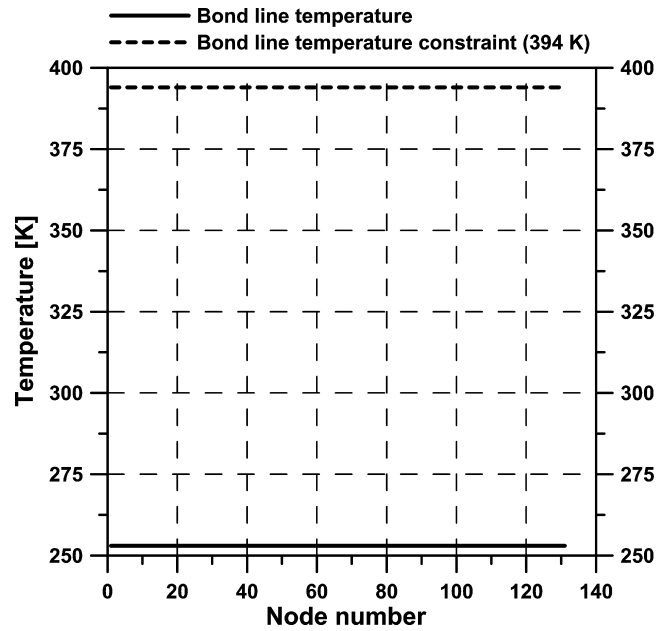


Fig. 19a. Final temperature on the bond-line nodes for ID 0.

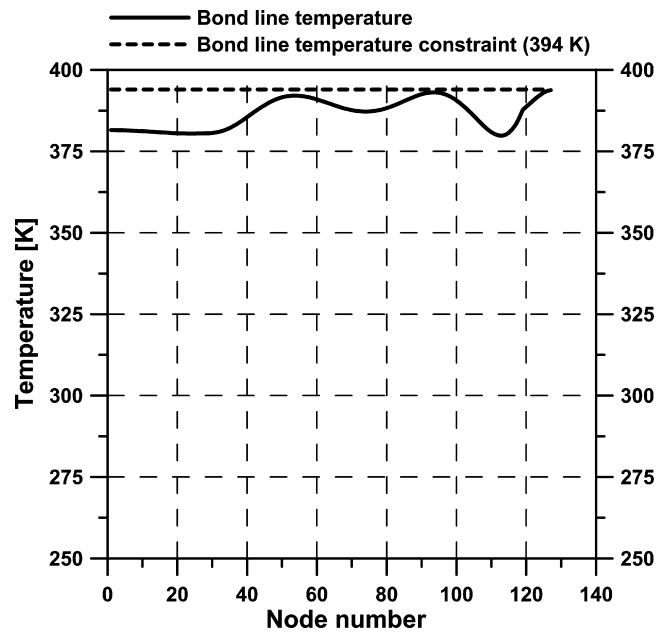


Fig. 19b. Final temperature on the bond-line nodes for ID 1336.

4. Numerical results

In this section, the results of the FE model optimization are shown. In particular, in Fig. 12, the object function variation versus the Design ID is shown. The minimum of the object function occurs for the individual “1336”.

As the individuals keep growing, they tend to concentrate along a certain path resulting in a stabilization of the objective function (see Fig. 12). Fig. 13 is a detail of Fig. 12 clearly showing the best estimated individual.

In Fig. 14 the values of maximum temperature on the bond-line (constraint function) for each ID are shown. In this case the values of the peak temperature tends to approach the limit set to 394 K [37,38], indicated in the Fig. 14 by the dotted line.

Fig. 15 shows the scatter matrix, representing the influence of optimization parameters on the analysis.

Scatter matrix shows how the variable sp9 (see Fig. 12) has more influence with respect to the other variables on the objective function. The ID “0” refers to the initial configuration while ID “1336” is the configuration with the lowest volume. In Figs. 16a

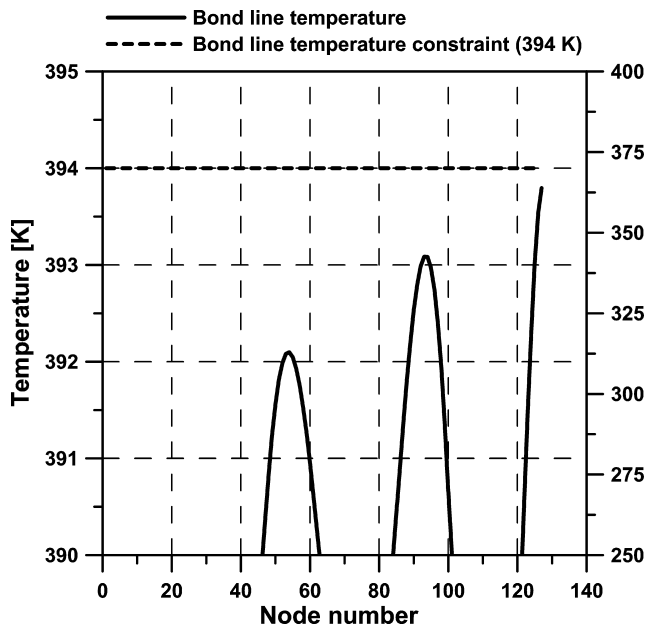


Fig. 20. Detail of Fig. 19b.

Table 4

Comparison between nominal and best configuration.

ID #	Volume (with margins) (m ³)	Peak temperature (K)	Volume reduction (-)
0	$3.841 \cdot 10^{-2}$	253.01	46%
1336	$2.070 \cdot 10^{-2}$	393.79	

and 16b, the initial configurations of the heat shields before entering the aero-thermic environment are shown.

Figs. 17a and 17b show the final configurations of the heat shields after exposure to the aero-thermic environment and the partial ablation of the heat shield.

In Figs. 18a and 18b, thermal profiles as nodal temperatures distribution (measured in Kelvin) after the thermal analysis are shown.

Figs. 19a and 19b show thermal profiles as temperature trends of the bond-line nodes after the analysis and the temperature bond-line limit [37,38].

In Fig. 20, a detail of Fig. 19b is shown.

In Fig. 19a the temperature values on the bond-line of the individual “0” is shown together with the constraint value. It is highlighted the marked gap between the two values. Fig. 19b, on the other hand, reports the same parameters for the best individual. In the second case, such gap is much less marked. Finally, in Fig. 20 a magnification of the regions where the differences are particularly low is reported. In Table 1 the values of the volume and of the temperature peak on the bond-line for the two configurations are shown. The Volume values reported in Table 4 have been obtained considering a margin of 22.1% on the thickness of the shield taking into account the trajectory margin, the aerothermal margin and the PICA material margin [38]. Considering this assumption, a volume reduction of 46% has been reached between the first and the optimum configuration.

5. Conclusions

In this paper a numerical model has been used to optimize the design of the ablative Thermal Protection System for the re-entry probe Stardust. Thanks to the numerical model, it was possible to

study the ablation phenomenon on the ablative heat shield. In particular, the numerical analysis consists in a FE model allowing to estimate the surface and bond-line temperatures and the final thickness of the ablative shield. Thanks to an optimization algorithm, the lowest ablative volume configuration, respecting the imposed temperature constrain, has been found. By comparing initial and best configurations, a 46% volume reduction resulted.

References

- [1] A. Ayasoufi, R.K. Rahmani, G. Cheng, R. Koomulli, Numerical simulation of ablation for reentry vehicles, 9th AIAA/ASME joint thermo-physics and heat transfer conference (2006) 2908.
- [2] J.H. Koo, D.W. Ho, O.A. Ezekoye, A review of numerical and experimental characterization of thermal protection material – Part I Numerical modelling, 42nd AIAA/ASME/SAE/ASEE joint propulsion conference & exhibit (2006).
- [3] R.D. Mathieu, Mechanical spallation of charring ablators in hyper-thermal environments, AIAA J. 2 (9) (1964).
- [4] R.L. Rockets, Potts Application of integral methods to ablation charring erosion, a review, J. Spacecr. 32 (2) (1995).
- [5] R.K. Clark, Simulation of pyrolysis-gas flow through a char layer during ablation. NASA TN D-5464 (1969).
- [6] E. Venkatapathy, C.E. Szalai, B. Laub, H. Hwang, J.L. Conley, J. Arnold, Thermal protection system technologies for enabling future sample return missions, NASA ARC, UC Santa Cruz, 2009.
- [7] P.N. Desai, D.T. Lyons, J. Tooley, J. Kangas, Entry, descent, and landing operations analysis for the stardust re-entry capsule. AIAA technical report (2006) 6410.
- [8] H.K. Tran et al., Phenolic impregnated carbon ablators (PICA) as thermal protection systems for discovery missions, NASA Technical Memorandum 110440 (1997).
- [9] L.R. Jackson, S.C. Dixon, A design assessment of multiwall, metallic standoff, and RSI reusable thermal protection systems including space shuttle application. NASA TM X-81780 (1980).
- [10] Y.I. Dimitrienko, Thermomechanics of composites under high temperatures, G. M.L. Gladwel, 1995.
- [11] M.B. Dow, R.T. Swann, S.S. Tompkins, Analysis of the effects of environmental conditions on the performance of charring ablators, J. Spacecr. Rockets 3 (1) (1966) 61–67.
- [12] V. Jones, K.N. Shukla, In-depth response of charring ablators to high temperature environment”, AIAA thermophysics conf., 33rd, Norfolk, VA (1999).
- [13] H. Mohammadiun, A. Kianifar, Numerical modeling of non-charring material ablation with considering chemical reaction effects, mass transfer and surface heat transfer, Eur. J. Sci. Res. 54 (3) (2011) 435–447.
- [14] R.P. Nathan, S. Bindu, Low temperature ablative heat shield for re-entry vehicles, 38th AIAA thermo-physics conference paper (2005) 5063.
- [15] G. Selvaduray, M. Cox, Annual report thermal protection materials development, Department of materials engineering, San Jose State University, CA 95192–0086, (1997) 1998.
- [16] F. Chavez, J. Agrawal, Fracture in phenolic impregnated carbon ablator, J. Spacecr. Rockets 50 (4) (2011) 1–7.
- [17] S.D. Williams, D.M. Curry, Thermal protection materials – thermophysical property data. Technical report RP-1289, NASA (1992).
- [18] J.A. Dec, R.D. Braun, An approximate ablative thermal protection system sizing tool for entry system design. 44th AIAA aerospace sciences meeting and exhibit. Reno, Nevada (2006).
- [19] F.S. Milos, Y. Chen, T.H. Squire, Updated ablation and thermal response program for spacecraft heatshield analysis, in: Proceedings of the 17th thermal and fluids analysis workshop, University of Maryland (1999).
- [20] H.K. Tran, C.E. Johnson, D.J. Rasky, F.C.L. Hui, M.T. Hsu, Y.K. Chen, D. Paragas, L. Kobayash, Phenolic impregnated carbon ablators (pica) as thermal protection systems for discovery missions, technical report TM-110440, NASA (1997).
- [21] V. Carandente, R. Scigliano, V. De Simone, A. Del Vecchio, R. Gardi, A Finite element approach for the design of innovative ablative materials for space applications. 6th European conference for aeronautics and space sciences (EUCASS). Krakow, Poland (2015).
- [22] R. Scigliano, M. Sionti, P. Lardeur, Verification, validation and variability for the vibration study of a car windshield modeled by finite elements, Finite elements in analysis and design, doi:10.1016/j.finel.2010.07.009.
- [23] W.L. Oberkampf, T.G. Trucano, C. Hirsch, Verification, validation, and predictive capability in computational engineering and physics, Appl. Mech. Rev. 57 (5) (2004) 345–384.
- [24] Thacker B.H., The role of nondeterminism in verification and validation of computational solid mechanics models, in: Proceedings of the 2003 SAE World Congress, Detroit, USA, 2003, ref. 2003–01-1353.
- [25] Matlab, Inch., Matrix Laborator Guide, Release 2010b (2010).
- [26] Ansys, Inch., Ansys Parametric Design Language Guide, Release 14.0 (2011, Nov.).
- [27] M.A. Covington, Performance of a light-weight ablative thermal protection material for the stardust mission sample return capsule, in: 2nd International planetary probe workshop (2004).

- [28] D.E. Goldberg, Genetic algorithms in search, optimization and machine learning, Addison-Wesley, 1989.
- [29] L. Chambers, Practical handbook of genetic algorithms. I, II CRC Press, (1995).
- [30] J.M. Holland, Adaptation in natural and artificial systems, MIT Press, 1995.
- [31] P.N. Desai, R.A. Mitcheltree, Cheatwood F. McNeil, Entry trajectory issues for the stardust sample return capsule, International Symposium on Atmospheric Reentry Vehicles and Systems Arcachon, France, 1999.
- [32] J.D. Anderson, Hypersonic and high temperature gas dynamics, McGraw-Hill, 1989.
- [33] K. Sutton, R.A. Graves, A general stagnation-point convective-heating equation for arbitrary gas mixtures. NASA TR R-376 (1971).
- [34] V. Carandente, R. Savino, Aerothermal analysis of a sample-return reentry capsule, FDMP 9 (4) (2013) 461–484.
- [35] M.E. Tauber, K. Sutton, Stagnation-point radiative heating relations for earth and mars entries, J. Spacecr. 28 (1) (1991) 40–42.
- [36] A. Viviani, G. Pezzella, Computational flowfield analysis of a planetary entry vehicle, numerical simulations - examples and applications in computational fluid dynamics, Lutz Angermann, ISBN: 978-953-307-153-4, (2010) (Chapter 7).
- [37] I. Cozmuta, D.B. Hash, D.A. Kontinos, Application of CEV sizing process of PICA to stardust and MSL, 7th International planetary probe workshop. Barcelona, Spain (2010).
- [38] I. Cozmuta, M.J. Wright, B. Laub, Defining ablative thermal protection system margins for planetary entry vehicles. 42nd AIAA thermophysics conference, Honolulu, Hawaii (2011).
- [39] Esteco. modeFrontier 4.3 user manual, (2010).